Relativistic description of electron Bernstein waves

J. Decker and A.K. Ram

October 2006

Plasma Science and Fusion Center
Massachusetts Institute of Technology
Cambridge MA 02139 USA

Relativistic description of electron Bernstein waves

Joan Decker

CEA/DSM/DRFC, Cadarache, 13108 Saint Paul lez Durance, France

Abhay K. Ram

MIT/PSFC, Cambridge, MA 02139, U.S.A.

(Dated: October 18, 2006)

The application of the extraordinary and ordinary electron cyclotron waves for heating and current drive in overdense, magnetized plasmas is restricted. For frequencies near low harmonics of the electron cyclotron frequency these waves are cutoff near the edge of the plasma. For higher frequencies the interaction of the waves with electrons is weak leading to very low absorption of wave power. However, electron Bernstein waves provide means for heating and current drive in overdense plasmas since they have no density cutoffs and are strongly damped near harmonics of the electron cyclotron resonance. This paper discusses properties of electron Bernstein waves that make them an attractive means for delivering energy and momentum to electrons. An approximate analytical model for electrostatic waves in the weakly relativistic and weak damping limits is developed. From this model the propagation and damping characteristics of electron Bernstein waves and their dependence on plasma parameters are derived. It is found that relativistic effects are necessary to properly describe the resonant interaction of electron Bernstein waves with electrons. The characteristics of electron Bernstein wave propagation and damping are very different depending on whether the electron cyclotron harmonic resonance is approached from the low- or the high-field side. The results from the analytical model and the associated analysis agree well with the results from the exact numerical calculations. This validates the physics of the simplifying assumptions on which the model is based. The electron Bernstein waves are completely damped well before the electron cyclotron resonance due to the Doppler shift. Within the damping region the waves interact with suprathermal electrons thereby having the potential for efficient current drive.

I. INTRODUCTION

In a magnetized plasma there are three types of linear waves that can propagate in the electron cyclotron (EC) range of frequencies: the extraordinary X modes, the ordinary O modes, and the electron Bernstein waves (EBW). The X and O modes are electromagnetic waves that can propagate in vacuum and have been used in conventional tokamaks for heating and current drive. However, their use is essentially limited to plasmas in which the electron plasma angular frequency ω_p is smaller than or comparable to the EC angular frequency ω_c. In very overdense plasmas where $\omega_p \gg \omega_c$ in the core, lower frequency X and O modes with angular frequency $\omega \sim \omega_c$ are cut-off near the edge of the plasma. Higher frequency X and O modes with $\omega \gtrsim \omega_p$ can access the core of the plasma but do not effectively damp on electrons because the resonant interaction between electrons and these electromagnetic modes is remarkably weak above the second harmonic of the EC frequency.

The EBWs are mostly electrostatic modes that do not propagate in vacuum and are excited in a plasma primarily by mode conversion of the X mode at the upper hybrid resonance. After excitation the EBWs propagate towards the core of the plasma without encountering density cut-offs. EBWs interact strongly with electrons in the vicinity of the Doppler shifted EC resonance or its harmonics. Thus, EBWs are strong candidates for delivering external energy and momentum to electrons in regions of a plasma inaccessible to the X and O modes [1] [2]. Coupling to EBWs via mode conversion has been demonstrated in stellarators [3] and tokamaks [4]. The same experiments have also seen effective interaction of EBWs with electrons. EBWs are particularly suitable for heating and current drive in the high-β plasmas of spherical tori like the National Spherical Torus Experiment (NSTX) [5] and the Mega Amp Spherical Tokamak (MAST) [6], where $\omega_p \gg \omega_c$ over most of the plasma.

There have been a number of theoretical works on the EBW dispersion relation [7] [8] [9], on mode conversion to EBWs [10] [11] [12], on emission of EBWs [13], and on current drive by EBWs [14]. However, a detailed study of the characteristics of EBWs and their resonant interaction with electrons has been lacking. Such study would be helpful in setting up EBW heating and current drive experiments. Providing a description of EBW characteristics and damping is the aim of this paper, which shows the role of relativistic effects in the interaction of EBWs with electrons.

The paper is organized as follows. In Section II the linear kinetic theory of high frequency waves in a relativistic plasma is developed. The conservation of wave energy density is formulated within the weak damping approximation. The theory is applied to the particular case of electrostatic waves. The resonant wave-particle interactions are discussed. Using a weakly relativistic approximation in a Maxwellian plasma, analytical expressions for the dispersion relation, the energy flow density, and the density of power dissipated are derived for obliquely propagating waves. In Section III the formalism of Section II is applied to electron Bernstein waves. The approximations used in Section II are justified by comparing the results obtained from the analytical model with the numerical results obtained from the code R2D2 [15] which calculates the exact relativistic linear wave characteristics. The EBW dispersion characteristics, their polarization, the associated energy flow density, and the density of power absorbed are calculated as a function of various plasma and wave parameters. In section IV the damping of EBWs approaching an EC harmonic resonance is calculated in a slab geometry. Analytic expressions for the power deposition profile are derived. The localization and width of the deposition region are determined both in momentum and in configuration spaces.

II. LINEAR KINETIC THEORY OF HIGH-FREQUENCY PLASMA WAVES

A. Linear high-frequency waves in a relativistic kinetic plasma

The linearized response of an infinite, uniform, static, magnetized plasma to a small-amplitude electromagnetic field expressed in space-time coordinates by $\mathcal{E}(\mathbf{r}, t) = \mathrm{Re}\left[\mathbf{E} \exp\left(i\mathbf{k} \cdot \mathbf{r} - i\omega t\right)\right]$ is determined from the conductivity tensor σ relating the current density $\mathbf{J} = \sigma \cdot \mathbf{E}$ to the electric field Fourier component $\mathbf{E}$ associated with the wave vector $\mathbf{k}$ and the angular frequency ω. The conductivity tensor is obtained from the linearized Vlasov equation [7]. For high frequency waves , where ω is in the EC frequency range, the ion dynamics can be ignored.

Starting from a cartesian coordinates system (x, y, z) defined such that the ambient magnetic field is $\mathbf{B} = B\widehat{\mathbf{z}}$ and the wave vector is $\mathbf{k} = k_\perp \widehat{\mathbf{x}} + k_\parallel \widehat{\mathbf{z}}$, a vector field $\mathbf{E}$ can be expressed in the rotating coordinates system

$$E_+ = \frac{E_x + iE_y}{\sqrt{2}}, \qquad E_- = \frac{E_x - iE_y}{\sqrt{2}}, \qquad E_\parallel = E_z \tag{1}$$

In this system, the conductivity tensor for a relativistic kinetic plasma [15] is

$$\sigma(\mathbf{k}, \omega) = i\varepsilon_0 \omega_p^2 \left\langle \sum_{n=-\infty}^{+\infty} \frac{p_\perp^2}{\gamma} \frac{1}{\left(\omega\gamma - k_\parallel c\beta_T p_\parallel - n\omega_c\right)} \mathbf{J}_n \mathbf{J}_n f_0 \right\rangle \tag{2}$$

where $\langle \cdots \rangle = 2\pi \int_0^\infty p_\perp \, dp_\perp \int_{-\infty}^\infty dp_\parallel$ denotes the momentum-space average. The momentum $\mathbf{p} = p_\parallel \widehat{\mathbf{z}} + \mathbf{p}_\perp$ is normalized to the thermal momentum $p_T = \sqrt{m\kappa T}$ where T is the electron temperature. Here $p_\perp = \|\mathbf{p}_\perp\|$, $\gamma = \sqrt{1 + \beta_T^2\left(p_\perp^2 + p_\parallel^2\right)}$, $\beta_T^2 \equiv \kappa T/\left(mc^2\right) = p_T^2/\left(mc\right)^2$, and $\mathbf{J}_n = \left(J_{n+1}/\sqrt{2}, J_{n-1}/\sqrt{2}, J_n p_\parallel/p_\perp\right)$ where J_n is the Bessel function of the first kind of order n and argument $\varsigma = \beta_T p_\perp k_\perp c/\omega_c$. The electron cyclotron and plasma angular frequencies are defined as $\omega_c = eB/m$ and $\omega_p = \sqrt{n_e e^2/m\varepsilon_0}$, respectively, where n_e is the electron density and m is the electron mass. The space-time independent, equilibrium electron distribution function $f_0\left(p_\perp, p_\parallel\right)$ must satisfy the three following normalized moments equations: $\langle f_0 \rangle = 1$, $\langle \mathbf{p} f_0 \rangle = \mathbf{0}$, and $\langle p^2 f_0/\gamma \rangle = 3$. The zero-order moment is the normalization, the first-order moment expresses the absence of zero-order current, and the second-order moment defines the electron temperature.

Including $\mathbf{J} = \sigma \cdot \mathbf{E}$ in Maxwell's equation, an equation for the self-consistent fields is obtained

$$\mathbb{D} \cdot \mathbf{E} = \mathbf{0} \tag{3}$$

where $\mathbb{D} = \mathbf{nn} - \left(\mathbf{n} \cdot \mathbf{n}\right)\mathbb{I} + \mathbb{K}$ is the dispersion tensor, and $\mathbf{n} = \mathbf{k}c/\omega$ is the wave index of refraction. $\mathbb{K} = \mathbb{I} + i/\left(\varepsilon_0 \omega\right)\sigma$ is the permittivity tensor

$$\mathbb{K} = \mathbb{I} - \frac{\omega_p^2}{\omega^2}\left\langle \sum_{n=-\infty}^{+\infty} \frac{p_\perp^2}{\gamma} \frac{1}{\left(\gamma - n_\parallel \beta_T p_\parallel - y_n\right)} \mathbf{J}_n \mathbf{J}_n f_0 \right\rangle \tag{4}$$

where $y_n = n\omega_c/\omega$ and $\mathbb{I}$ is the unit tensor. Non-trivial solutions to the wave equation are obtained if the dispersion relation

$$\det \mathbb{D} \equiv D\left(\omega, n_\perp, n_\parallel\right) = 0 \tag{5}$$

is satisfied. For prescribed ω and $n_\parallel$, the dispersion relation solves for $n_\perp = n_\perp\left(n_\parallel, \omega\right)$. The corresponding electric field polarization vector defined by $\mathbf{e} = \mathbf{E}/\|\mathbf{E}\|$ is then determined from (3).

B. Weak damping approximation

It is assumed that ω and $n_\parallel$ are prescribed real quantities. In general, the solution to the dispersion relation (5) leads to complex $n_\perp\left(n_\parallel, \omega\right) = n_{\perp r} + i n_{\perp i}$ where $n_{\perp r}$ and $n_{\perp i}$ are the real and imaginary parts of $n_\perp$, respectively. The dispersion tensor can be expressed as $\mathbb{D} = \mathbb{D}^{\mathrm{H}} + i\mathbb{D}^{\mathrm{A}}$ where $\mathbb{D}^{\mathrm{H}} = \left(\mathbb{D} + \mathbb{D}^\dagger\right)/2$ and $\mathbb{D}^{\mathrm{A}} = \left(\mathbb{D} - \mathbb{D}^\dagger\right)/2i$ are the hermitian and the antihermitian parts of $\mathbb{D}$, respectively.

The weak damping approximation assumes $|\mathbb{D}_{ij}^{\mathrm{A}}| \ll |\mathbb{D}_{ij}^{\mathrm{H}}|$. Taking $\epsilon \sim |\mathbb{D}_{ij}^{\mathrm{A}}|/|\mathbb{D}_{ij}^{\mathrm{H}}| \ll 1$ as a small expansion parameter, the perpendicular index of refraction, polarization and dispersion tensor can be expressed as

$$\begin{aligned} n_\perp &= n_{\perp 0} + n_{\perp 1} + \cdots \\ \mathbf{e} &= \mathbf{e}_0 + \mathbf{e}_1 + \cdots \\ \mathbb{D} &= \mathbb{D}\left(n_{\perp 0}\right) + n_{\perp 1}\left.\frac{\partial \mathbb{D}}{\partial n_{\perp r}}\right|_{n_\perp = n_{\perp 0}} + \cdots \end{aligned} \tag{6}$$

where elements with subscript $m = 0, 1, \cdots$ are of order ϵ^m and the Taylor expansion of $\mathbb{D}$ is possible because $\mathbb{D}\left(n_\perp\right)$ is analytical. Upon substituting (6) in (3) the wave equation can be ordered in powers of ϵ. To order ϵ^0 we obtain

$$\mathbb{D}^{\mathrm{H}}\left(n_{\perp 0}\right) \cdot \mathbf{e}_0 = \mathbf{0} \tag{7}$$

and the corresponding dispersion relation

$$\det\left[\mathbb{D}^{\mathrm{H}}(n_{\perp 0})\right] \equiv D_{\mathrm{H}}\left(\omega, n_{\perp 0}, n_\parallel\right) = 0 \tag{8}$$

can be solved for $n_{\perp 0} = n_{\perp 0}\left(n_\parallel, \omega\right)$. For propagating modes $n_{\perp 0} = n_{\perp r0}$ is real since $\mathbb{D}^{\mathrm{H}}$ is hermitian. The electric field polarization $\mathbf{e}_0$ is then determined from (7). To order ϵ^1 we obtain

$$\mathbb{D}^{\mathrm{H}}\left(n_{\perp 0}\right) \cdot \mathbf{e}_1 = -\left[i\mathbb{D}^{\mathrm{A}}\left(n_{\perp r0}\right) + n_{\perp 1}\left.\frac{\partial \mathbb{D}^{\mathrm{H}}}{\partial n_{\perp r}}\right|_{n_\perp = n_{\perp r0}}\right] \cdot \mathbf{e}_0 \tag{9}$$

Since $\det[\mathbb{D}^{\mathrm{H}}(n_{\perp 0})] = 0$ (9) implies

$$\mathbf{e}_0^* \cdot \left[i\mathbb{D}^{\mathrm{A}}(n_{\perp r0}) + n_{\perp 1} \left. \frac{\partial \mathbb{D}^{\mathrm{H}}}{\partial n_{\perp r}} \right|_{n_\perp = n_{\perp r0}} \right] \cdot \mathbf{e}_0 = 0 \tag{10}$$

Subtracting (10) from its complex conjugate yields

$$\mathbf{e}_0^* \cdot \left[\mathbb{D}^{\mathrm{A}}(n_{\perp r0}) + n_{\perp i1} \left. \frac{\partial \mathbb{D}^{\mathrm{H}}}{\partial n_{\perp r}} \right|_{n_\perp = n_{\perp r0}} \right] \cdot \mathbf{e}_0 = 0 \tag{11}$$

which can be solved for $n_{\perp i1}$

$$n_{\perp i1} = -\frac{\mathbf{e}_0^* \cdot \mathbb{D}^{\mathrm{A}}(n_{\perp r0}) \cdot \mathbf{e}_0}{\mathbf{e}_0^* \cdot (\partial \mathbb{D}^{\mathrm{H}}/\partial n_{\perp r})_{n_\perp = n_{\perp r0}} \cdot \mathbf{e}_0} \tag{12}$$

In the rest of this paper, the weak damping approximation is assumed. The perpendicular component of the index of refraction $\mathbf{n}$ is $n_{\perp 0}$ determined from (8) such that $\mathbf{n}$ is real, and the polarization $\mathbf{e}$ is $\mathbf{e}_0$ determined from (7).

C. Wave energy conservation

In the weak damping approximation, the steady-state equation for wave energy conservation is obtained by letting the wave field amplitudes be a slowly varying functions of space [16]

$$\mathcal{E}(\mathbf{r}, t) = \mathrm{Re}\left[\mathbf{E}(\mathbf{r}) \exp(i\mathbf{k} \cdot \mathbf{r} - i\omega t) \right] \tag{13}$$

with

$$|\nabla_i E_j| \ll |k_i E_j| \tag{14}$$

This leads to the time-averaged wave energy conservation equation [16] [17]

$$\nabla \cdot \mathbf{S} + P = 0 \tag{15}$$

where

$$\mathbf{S} = -\frac{\varepsilon_0 c}{4} \|\mathbf{E}\|^2 \frac{\partial}{\partial \mathbf{n}} \left(\mathbf{e}^* \cdot \mathbb{D}^{\mathrm{H}} \cdot \mathbf{e} \right) \tag{16a}$$

$$P = \frac{\varepsilon_0 \omega}{2} \|\mathbf{E}\|^2 \left(\mathbf{e}^* \cdot \mathbb{K}^{\mathrm{A}} \cdot \mathbf{e} \right) \tag{16b}$$

$\mathbf{S}$ is the time-averaged energy flow density associated with the wave and P is the time-averaged density of power dissipated. In a kinetic plasma, $\mathbf{S}$ includes both the electromagnetic energy flow density, or Poynting flow, and the kinetic energy density of particles moving coherently in the electromagnetic wave. In the cold plasma limit, the latter contribution to $\mathbf{S}$ vanishes. The expressions (16) for $\mathbf{S}$ and P are divided by the square of the electric field amplitude to obtain the normalized quantities

$$\overline{\mathbf{S}} \equiv \frac{\mathbf{S}}{(\varepsilon_0 c/2) \|\mathbf{E}\|^2} = -\frac{1}{2} \frac{\partial}{\partial \mathbf{n}} \left(\mathbf{e}^* \cdot \mathbb{D}^{\mathrm{H}} \cdot \mathbf{e} \right) \tag{17a}$$

$$\overline{P} \equiv \frac{P}{(\varepsilon_0 \omega/2) \|\mathbf{E}\|^2} = \mathbf{e}^* \cdot \mathbb{K}^{\mathrm{A}} \cdot \mathbf{e} \tag{17b}$$

In terms of the permittivity tensor

$$\overline{\mathbf{S}} = -\frac{1}{2} \frac{\partial}{\partial \mathbf{n}} \left[|\mathbf{n} \cdot \mathbf{e}|^2 - \|\mathbf{n}\|^2 + \mathbf{e}^* \cdot \mathbb{K}^{\mathrm{H}} \cdot \mathbf{e} \right] \tag{18}$$

For an electromagnetic wave in vacuum, $\mathbf{n} \cdot \mathbf{e} = 0$, $\|\mathbf{n}\| = 1$ and $\mathbb{K}^{\mathrm{H}} = 0$ so that $\overline{\mathbf{S}} = \widehat{\mathbf{L}}$ where $\widehat{\mathbf{L}} \equiv \mathbf{n}/\|\mathbf{n}\|$ is in the direction of the wave vector.

The momentum space integrand in (4) has a pole on the real $p_\parallel$ axis. Thus, the integral over $p_\parallel$ leads to a principal value integral and a resonant contribution. For a non-relativistic Maxwellian plasma this decomposition into principal value and resonant term is contained in the usual plasma dispersion function. The energy propagation is associated with the non-resonant term

$$\mathbf{e}^* \cdot \mathbb{K}^{\mathrm{H}} \cdot \mathbf{e} = 1 - \frac{\omega_p^2}{\omega^2} \mathcal{P} \left\langle \sum_{n=-\infty}^{+\infty} \frac{p_\perp^2}{\gamma} \frac{|\Theta|^2}{\left(\gamma - n_\parallel \beta_T p_\parallel - y_n\right)} f_0 \right\rangle \tag{19}$$

where $\mathcal{P}$ denotes the principal value integral. The power absorption is associated with the resonant term

$$\overline{P} = \pi \frac{\omega_p^2}{\omega^2} \left\langle \sum_{n=-\infty}^{+\infty} \frac{p_\perp^2}{\beta_T} \frac{|\Theta|^2}{\left|\gamma n_\parallel - \beta_T p_\parallel\right|} \delta\left(p_\parallel - p_{\parallel \mathrm{res}}\right) f_0 \right\rangle \tag{20}$$

where the resonance condition

$$\gamma\left(p_\perp, p_\parallel\right) - n_\parallel \beta_T p_\parallel - y_n = 0 \tag{21}$$

is formally written as $p_\parallel = p_{\parallel \mathrm{res}}(p_\perp)$. In (19) and (20) Θ is given by

$$\Theta = \mathbf{J}_n \cdot \mathbf{e} = \frac{J_{n+1}}{\sqrt{2}} e_+ + \frac{J_{n-1}}{\sqrt{2}} e_- + \frac{p_\parallel}{p_\perp} J_n e_\parallel \tag{22}$$

It has been shown [18] that the rate of change of electrons kinetic energy density obtained from the quasilinear electromagnetic wave diffusion operator [19][20] gives the same expression as (20) for a uniform relativistic Maxwellian plasma. The form (20) is interesting for numerical calculations of fully relativistic damping since the delta function reduces the momentum-space integrals to a single integral over $p_\perp$.

The perpendicular absorption coefficient is defined as

$$\alpha_\perp = \frac{P}{S_\perp} = \frac{\omega}{c} \frac{\overline{P}}{\overline{S}_\perp} \tag{23}$$

where $\overline{S}_\perp = \overline{\mathbf{S}} \cdot \hat{\mathbf{x}}$. $\alpha_\perp$ is independent of the wave electric field amplitude and is a function of $(\omega, \mathbf{k})$ and the local plasma parameters. The absorption coefficient is related to the imaginary part of the wave vector. From (12), (16) and (23) $\alpha_\perp = 2\omega n_{\perp i}/c = 2\,\mathrm{Im}\,[k_\perp]$. This illustrates the self-consistency of the ordering scheme used in the weak damping approximation.

D. Electrostatic dispersion relation

The wave equation (7) can be expressed in the in the (T_1, T_2, L) coordinate system, where $\hat{\mathbf{L}} = \mathbf{n}/\|\mathbf{n}\|$ is the longitudinal unit vector, and $\hat{\mathbf{T}}_2 = \hat{\mathbf{y}}$ and $\hat{\mathbf{T}}_1 = \hat{\mathbf{y}} \times \hat{\mathbf{L}}$ lie in the plane perpendicular to the wave vector. With $\mathbf{e} = e_L \hat{\mathbf{L}} + \mathbf{e}_T$ (7) becomes

$$e_L \mathbb{K}^{\mathrm{H}} \cdot \hat{\mathbf{L}} + \left(\mathbb{K}^{\mathrm{H}} - \|\mathbf{n}\|^2 \mathbb{I}\right) \cdot \mathbf{e}_T = 0 \tag{24}$$

For $\|\mathbf{n}\|^2 \gg \left|K_{ij}^{\mathrm{H}}\right|$ (24) is approximately

$$\mathbf{e}_T \simeq \frac{e_L}{\|\mathbf{n}\|^2} \mathbb{K}^{\mathrm{H}} \cdot \hat{\mathbf{L}} \tag{25}$$

Thus $\|\mathbf{e}_T\| \ll |e_L|$ and $\mathbf{e} \simeq \hat{\mathbf{L}}$.

From (25) the electrostatic dispersion relation is derived

$$D_{\mathrm{L}}\left(\omega, \mathbf{n}\right) \equiv \hat{\mathbf{L}} \cdot \mathbb{K}^{\mathrm{H}} \cdot \hat{\mathbf{L}} = 0 \tag{26}$$

The same dispersion relation can also be obtained by solving the Poisson-Vlasov system for linear electrostatic waves [17]. Since the polarization $\mathbf{e} = \hat{\mathbf{L}}$ is electrostatic, the contribution of the Poynting flow to $\overline{\mathbf{S}}$ vanishes, so that (18) reduces to

$$\overline{\mathbf{S}}_{\mathrm{L}} = -\frac{1}{2} \frac{\partial D_{\mathrm{L}}\left(\omega, \mathbf{n}\right)}{\partial \mathbf{n}} \tag{27}$$

and Θ (22) takes the form

$$\Theta_{\mathrm{L}} = \mathbf{J}_n \cdot \widehat{\mathbf{L}} = \frac{\left(y_n + \beta_T n_\parallel p_\parallel\right)}{\sqrt{n_\parallel^2 + n_\perp^2}} \frac{J_n}{\beta_T p_\perp} \tag{28}$$

Substituting (28) in (19) and (20) yields an expression for the electrostatic dispersion relation (26)

$$D_{\mathrm{L}}\left(\omega, \mathbf{n}\right) = 1 - \frac{\omega_p^2}{\omega^2} \mathcal{P} \left\langle \sum_{n=-\infty}^{+\infty} \frac{J_n^2}{\gamma \left(n_\parallel^2 + n_\perp^2\right) \beta_T^2} \frac{\left(y_n + n_\parallel \beta_T p_\parallel\right)^2}{\left(\gamma - n_\parallel \beta_T p_\parallel - y_n\right)^2} f_0 \right\rangle \tag{29}$$

and the density of power absorbed

$$\overline{P}_{\mathrm{L}} = \pi \frac{\omega_p^2}{\omega^2} \left\langle \sum_{n=-\infty}^{+\infty} \frac{J_n^2}{\left(n_\parallel^2 + n_\perp^2\right) \beta_T^3} \frac{\left(y_n + n_\parallel \beta_T p_\parallel\right)^2}{\left|\gamma n_\parallel - \beta_T p_\parallel\right|} \delta\left(p_\parallel - p_{\parallel\mathrm{res}}\right) f_0 \right\rangle \tag{30}$$

E.   Resonant wave/electron interaction

The resonant interaction between electrons and the plasma waves is given by the resonance condition (21). The resonance curves defined in $(p_\perp, p_\parallel)$ momentum space are ellipses for $\left|n_\parallel\right| < 1$, parabolas for $\left|n_\parallel\right| = 1$, and hyperbolas for $\left|n_\parallel\right| > 1$. For $\left|n_\parallel\right| > 1$ there is always some part of momentum space in resonance with the waves. For $\left|n_\parallel\right| \leq 1$ the resonance curves exist provided

$$y_n = \frac{n\omega_c}{\omega} > \sqrt{1 - n_\parallel^2} \tag{31}$$

A particular point of interest on the wave-particle resonance curve is the one point that is closest to the origin $\left(p_\perp, p_\parallel\right) = (0, 0)$ in momentum space. For a Maxwellian distribution function this point would correspond to the maximum phase-space density of particles that interact with the plasma waves. This point of closest approach in momentum space will be useful in calculating the wave damping and determining the wave power deposition profile.

The coordinates $\left(p_{\perp\min}, p_{\parallel\min}\right)$ of this point are determined by minimizing the distance $\sqrt{p_\perp^2 + p_\parallel^2}$ to origin in momentum space, which gives

$$p_{\perp\min} = 0 \tag{32a}$$

$$p_{\parallel\min} = \begin{cases} \sigma_\parallel \dfrac{\left(\left|n_\parallel\right| y_n - \sqrt{y_n^2 + n_\parallel^2 - 1}\right)}{\beta_T\left(1 - n_\parallel^2\right)} & \text{for } n_\parallel \neq 1 \\[4mm] \sigma_\parallel \dfrac{\left(1 - y_n^2\right)}{2\beta_T y_n} & \text{for } n_\parallel = 1 \end{cases} \tag{32b}$$

where $\sigma_\parallel$ is the sign of $n_\parallel$. The point of closest approach, identified by $p_n \equiv p_{\parallel\min}$, is thus located on the $p_\perp = 0$ axis. It is found that $\sigma_\parallel p_n > 0$ in the low-field side (LFS) approach to the n's harmonic resonance ($y_n < 1$) and $\sigma_\parallel p_n < 0$ in the high-field side (HFS) approach to the n's harmonic resonance ($y_n > 1$). When $y_n = 1$, the wave is exactly at the n's harmonic resonance and $p_n = 0$. The point p_n moves closer to the origin as $y_n \to 1$.

On Fig.1 we show parabolic resonance curves ($n_\parallel = 1$) in momentum space for $y_n = 0.9$ (a) and $y_n = 1.1$ (b) corresponding respectively to a LFS and a HFS approach to the n's harmonic resonance. At the point p_n located on the $p_\perp = 0$ axis the resonance curves are closest to the origin in momentum space.

F.   Weakly relativistic approximation for obliquely propagating waves in a Maxwellian plasma

From here on we will assume that the electron distribution function is a relativistic Maxwellian

$$f_{\mathrm{M}} = \frac{R\left(\beta_T\right)}{(2\pi)^{3/2}} e^{-\frac{(\gamma - 1)}{\beta_T^2}} \tag{33}$$

where

$$R\left(\beta_T\right) = \sqrt{\frac{\pi}{2}} \frac{\beta_T}{K_2\left(1/\beta_T^2\right)} e^{-\frac{1}{\beta_T^2}} \tag{34}$$

and K_2 is the modified Bessel function of the second kind and second order.

Unlike the non-relativistic calculations [8], the dispersion relation (29) and density of power dissipated (30) can no longer be expressed in terms of any standard functions. They have to be computed numerically [15]. The code R2D2 solves the fully relativistic dispersion relation (5) in the EC range of frequencies and calculates the wave polarization, energy flow density, and density of power dissipated.

An analytical analysis can be carried out in the weakly relativistic limit, $\beta_T \ll 1$, for the case of obliquely propagating waves with $|n_\parallel| \gg \beta_T$. Then from (32b)

$$p_n = p_{n0}\left[1 + \frac{\beta_T p_{n0}}{2n_\parallel}\right] \tag{35}$$

where

$$p_{n0} = \frac{1 - y_n}{\beta_T n_\parallel} \tag{36}$$

is the non-relativistic limit of p_n and is the Doppler shift of the resonance. The second term in (35) is the relativistic shift of the resonance. Equation (35) is obtained by substituting $y_n = 1 - \beta_T n_\parallel p_{n0}$ in (32b) and is valid for n such that $|p_{n0}| \ll |n_\parallel|/\beta_T$. The n for which $|p_{n0}| \gtrsim |n_\parallel|/\beta_T$ do not contribute to the wave damping.

The dispersion relation (29) and density of power absorbed (30) for electrostatic waves with $|n_\parallel| \gg \beta_T$ are calculated in Appendix A. We show that relativistic effects can be neglected in determining the wave vector, the polarization and the energy flow density. These quantities are related to the principal value of the momentum space integrals in the permittivity tensor. Thus, from (A14)

$$D_{\mathrm{L}} = 1 + \frac{\omega_p^2}{\omega_c^2} \sum_{n=-\infty}^{+\infty} \left[\frac{\Gamma_n\left(\lambda_\perp\right)}{\lambda} \left(1 + y_n + \zeta_0 \operatorname{Re}\left[Z\left(\zeta_n\right)\right]\right)\right] \tag{37}$$

where $Z\left(\zeta_n\right)$ is the usual plasma dispersion function, $\zeta_n \equiv \left(1 - y_n\right)/\left(\sqrt{2}\left|n_\parallel\right|\beta_T\right)$, $\lambda_\perp \equiv \left(n_\perp \beta_T \omega/\omega_c\right)^2$, $\lambda_\parallel \equiv \left(n_\parallel \beta_T \omega/\omega_c\right)^2$ and $\lambda \equiv \lambda_\parallel + \lambda_\perp$. Here, $\Gamma_n\left(\lambda_\perp\right) \equiv I_n\left(\lambda_\perp\right)e^{-\lambda_\perp}$ where I_n is the modified Bessel function of the first kind of order n.

In determining the wave damping we, however, have to retain relativistic corrections. Previous studies of the X and O modes have also noted the need to include relativistic effects in the resonance condition [21]. From (A20) we obtain

$$\overline{P}_{\mathrm{L}} = \sqrt{\frac{\pi}{2}} \frac{1}{\lambda\left|n_\parallel\right|\beta_T} \frac{\omega_p^2}{\omega_c^2} \sum_{\substack{n=-\infty \\ |p_{n0}|\ll|n_\parallel|/\beta_T}}^{+\infty} \left\{\Gamma_n\left(\lambda_\perp\right) - \frac{\beta_T p_{n0}}{n_\parallel}\left[\lambda_\perp \Gamma_n\left(\lambda_\perp\right)\right]'\right\} e^{-\frac{p_n^2}{2}} \tag{38}$$

$\overline{P}_{\mathrm{L}}$ includes the first order effects of both the relativistic shift through the term p_n (35), and the relativistic curvature through the second term in the (38). If we ignore the relativistic curvature and assume that $\lambda_\perp \gg \lambda_\parallel$, then

$$\overline{P}_{\mathrm{L}} = \sqrt{\frac{\pi}{2}} \frac{1}{\beta_T\left|n_\parallel\right|} \frac{\omega_p^2}{\omega_c^2} \sum_{n=-\infty}^{+\infty} \frac{\Gamma_n\left(\lambda_\perp\right)}{\lambda_\perp} e^{-\frac{p_n^2}{2}} \tag{39}$$

The density of power absorbed is proportional to the phase space density of electrons at the momentum space point p_n. This illustrates the significance of p_n, which is the point on the resonance curve that is closest to the origin.

Approximate expressions for D_{L} and $\overline{P}_{\mathrm{L}}$ can also be derived for nearly perpendicular propagation when $|n_\parallel| \ll \beta_T$. However, the region of power deposition, located on the high-field side of the resonance, is so close to the resonance that the polarization of wave is no longer electrostatic. Also, relativistic effects have to be included in the evaluation of D_{L}. These calculations are beyond the scope of this paper as we are primarily interested in addressing the propagation and damping of EBWs relevant to current drive, with $|n_\parallel| \gg \beta_T$.

III.   CHARACTERISTICS OF ELECTRON BERNSTEIN WAVES IN A MAXWELLIAN PLASMA

The formulation of section II for electrostatic waves is applied to electron Bernstein waves. The validity of the approximations used in this model is checked by comparing the results with those obtained from R2D2. As indicated earlier, R2D2 is a numerical code that calculates the characteristics of waves in the EC frequency range in a completely relativistic Maxwellian plasma [15]. R2D2 can also calculate wave characteristics in a non-relativistic Maxwellian plasma. The wave characteristics in a Maxwellian plasma are function of four normalized independent parameters: ω_p/ω, ω_c/ω, β_T, and $n_\parallel$. The results will be expressed in terms of these dimensionless parameters.

A.   Weak damping approximation for EBWs

Using R2D2 the perpendicular index of refraction $n_\perp$ is evaluated by solving the electromagnetic dispersion relation (5) for a fully relativistic Maxwellian plasma. In order to check the validity of the weak damping approximation, the real and imaginary parts of $n_\perp$ are compared to the solution of (8) and the expression (12), respectively. The results are displayed in Figs.2(a) and 2(b) where the real part $n_{\perp r}$ and the imaginary part $n_{\perp i}$, respectively, are plotted as a function of ω/ω_c between the first and second harmonics. The weak damping approximation breaks down near the EC harmonics where $|n_{\perp i}| \sim |n_{\perp r}|$.

In section IV we will show that, in their approach to an EC resonance, EBWs are completely damped in a region sufficiently far away from the resonance such that the weak damping approximation is valid. Also, in this region of interest, the argument ζ_n of the plasma dispersion function is sufficiently large ($|\zeta_n| \gtrsim 2$) so that the expansion $Z(\zeta_n) \simeq -1/\zeta_n$ is valid. For electrostatic waves with $\lambda_\perp \gg \lambda_\parallel$ the electrostatic dispersion relation (26) reduces to

$$D_{\mathrm{L}} = 1 - 2\frac{\omega_p^2}{\omega_c^2} \sum_{n=1}^{+\infty} \frac{\Gamma_n(\lambda_\perp)}{\lambda_\perp} \frac{y_n^2}{1 - y_n^2} = 0 \tag{40}$$

This equation, first derived by I. Bernstein [7], is a polynomial equation for $\omega(\lambda_\perp)$. It can be solved systematically and is used as an initial guess in more complicated calculations and in the R2D2 code. It is interesting to note that in its approximate form (40), the dispersion relation predicts that the normalized wave vector $k_\perp \rho_T = \sqrt{\lambda_\perp}$ be independent of the temperature and the parallel wave vector.

Using (40), the perpendicular energy flow density (27) $\overline{S}_{\mathrm{L}\perp} = \overline{\mathbf{S}}_{\mathrm{L}} \cdot \widehat{\mathbf{x}} = -(1/2)\,\partial D_{\mathrm{L}}/\partial n_\perp$ becomes

$$\overline{S}_{\mathrm{L}\perp} \simeq \beta_T \frac{\omega_p^2}{\omega_c^2} \Phi_\perp(\omega/\omega_c, \lambda_\perp) \tag{41}$$

where

$$\Phi_\perp(\omega/\omega_c, \lambda_\perp) \simeq 2\sqrt{\lambda_\perp}\, \frac{\omega}{\omega_c} \sum_{n=1}^{+\infty} \frac{y_n^2}{1 - y_n^2} \frac{\partial}{\partial \lambda_\perp}\left(\frac{\Gamma_n(\lambda_\perp)}{\lambda_\perp}\right) \tag{42}$$

is independent of the temperature and the parallel wave vector.

B.   Dispersion characteristics

In the weak damping approximation, the real part of $k_\perp \rho_T$, solution to the fully electromagnetic (EM) dispersion relation (8), is calculated using R2D2 in both the fully relativistic (FR) and the non-relativistic (NR) cases. The results are also compared to the non-relativistic, electrostatic (ES) solution of the approximate equation (40). In Fig.3 $k_\perp \rho_T$ is shown, between the first and second harmonics, as a function of various normalized plasma and wave parameters.

From Fig.3(a) we note that $k_\perp \rho_T$ depends strongly upon magnetic field variations. On the low field side near the $\omega/\omega_c = 1$ resonance, the wavelength tends to be shorter than the Larmor radius. On the high field side near the $\omega/\omega_c = 2$ resonance the wavelength tends to be larger than the Larmor radius. This property of EBWs holds true at higher harmonics. The difference between LFS and HFS wave characteristics affects the momentum space localization of the resonant wave-particle interaction.

The results in graphs Fig.3(b) and Fig.3(c) show that $k_\perp \rho_T$ does not vary much with temperature and $n_\parallel$. From Fig.3(d) we observe a strong dependence on the density near the mode-conversion region (MCR) in the vicinity of

the upper-hybrid resonance (UHR). However, $k_\perp \rho_T$ does not vary much with density far from the MCR. Figure 3(b) shows that the relativistic correction scales as β_T^2, which is expected from the results of section A 3. For plasma temperatures $T \leq 12$ keV, which corresponds to $\beta_T \leq 0.15$, the relativistic correction is less that than 15%.

The results in Figure 3 show that the electrostatic expression (40), which is independent of β_T and $n_\parallel$, is a good approximation to the dispersion relation except in the region near the EC resonances. In this region $|\zeta_n| \lesssim 2$ and the asymptotic expansion of the Z function is no longer valid.

C. Polarization

The polarization vector $\mathbf{e}$ in (7) is calculated using R2D2 for the relativistic and non-relativistic forms of the dispersion tensor. The components of $\mathbf{e}$ in the (T_1, T_2, L) coordinate system are shown in Fig.4(a) as a function of ω/ω_c, and in Fig.4(b) as a function of β_T, between the first and second harmonics. For electrostatic waves the polarization is longitudinal with $(e_{T1}, e_{T2}, e_L) = (0, 0, 1)$.

From the results in Fig.4 we note that the longitudinal component of the polarization is much larger than the transverse components. This validates the electrostatic approximation for the waves. The relativistic corrections in the polarization are of order β_T^2 and remain negligible for typical fusion plasma temperatures. The dependence of the polarization on $n_\parallel$ and on the normalized density ω_p^2/ω^2 were also determined. We found that the variations were negligibly weak except near the MCR.

D. Perpendicular energy flow density

The fully electromagnetic normalized perpendicular energy flow density $\overline{S}_\perp$ (18) is calculated using R2D2 for both the relativistic and non-relativistic cases. The results are compared with the approximate non-relativistic electrostatic form (41). The results are plotted in Fig.5. We note that the electrostatic expression (41) is a good approximation except near the EC resonances.

According to (17a), the inverse of $\overline{S}_\perp$ is a measure of the electric field amplitude per unit perpendicular energy flow density. For an electromagnetic wave propagating in vacuum $\overline{S}_\perp = 1$. Figure 5(a) shows that $\overline{S}_\perp \ll 1$ on the LFS and $\overline{S}_\perp \gtrsim 1$ on the HFS. Therefore, for a given energy flow density, the electric field amplitude is much larger on the LFS than on the HFS where it is comparable to the amplitude of electromagnetic X and O modes. Since the magnitude of resonant wave-particle interaction is proportional to $\|\mathbf{E}\|^2$ (16b), the approach to a resonance, from the HFS or the LFS, is important in determining the strength of this interaction.

It is shown in Fig.3 that $\lambda_\perp = (k_\perp \rho_T)^2$ is essentially independent of the temperature, the density (away from the MCR) and the parallel index of refraction. Then, from (41), $\overline{S}_\perp$ should increase linearly with ω_p^2/ω^2 and with β_T, and be independent of $n_\parallel$. These predictions are confirmed in Fig.5. This linear dependence with respect to β_T and ω_p^2/ω^2 is characteristic of electrostatic waves. For such waves the energy flow is due to the coherent motion of particles and, thus, is proportional to the density n_e and velocity $v_T = \beta_T c$ of the energy carriers.

The relativistic corrections increase as β_T^2 as seen in graph Fig.5(b). The corrections are of the same order as for the dispersion characteristics.

E. Density of power absorbed

In Fig.6 the normalized density of power absorbed $\overline{P}$ for an obliquely propagating EBW ($n_\parallel = 1$) is displayed as a function of ω/ω_c between the first and second harmonic. The electromagnetic relativistic and non-relativistic calculations of $\overline{P}$ (20) using the code R2D2 are compared with the approximate electrostatic expression (39) where p_n is given by the weakly relativistic (WR) and non-relativistic limits in (35) and (36), respectively.

These results show the importance of relativistic effects in evaluating the power absorbed by electrons. The weakly relativistic formalism properly accounts for the relativistic effect, which is primarily the shift in the resonance condition included in p_n (35). The relativistic correction leads to a decrease in the absorption for the LFS approach and an increase for the HFS approach to a resonance.

The differences between the results from R2D2 and from (39) occur in the same region where the asymptotic approximation to the plasma dispersion function breaks down. As indicated before, the EBWs are completely damped before the weak damping approximation becomes invalid.

IV. EBW POWER DEPOSITION PROFILE

In this section we calculate the power deposition profile of an EBW propagating toward an EC harmonic resonance. There are two reasons for this calculation. The first reason is to show that the EBWs are completely damped on electrons before the weak damping approximation breaks down. The second reason is important from a practical point of view. If EBWs are to be used for heating or for driving plasma currents it is necessary to know the extent, in configuration space and in momentum space, over which the EBWs will deposit their energy and momentum.

We consider a slowly varying plasma in which the typical scale length L of variations in the equilibrium quantities (the magnetic field, the temperature, and the density) is much larger than the wavelength $2\pi/k$ of the wave. Then the WKB approximation is valid and the propagation characteristics of the wave are determined by the local plasma parameters. We assume a slab geometry with plasma inhomogeneities along the x direction perpendicular to the magnetic field. This geometry is a good representation of a wave propagating along the horizontal mid-plane in a toroidal plasma. In this case the parallel index of refraction $n_\parallel$ is constant and independent of the plasma parameters.

From (15) the energy conservation equation is

$$\frac{dS_\perp}{dx} + P = 0 \tag{43}$$

From (43) and (23)

$$\alpha_\perp = -\frac{1}{S_\perp}\frac{dS_\perp}{dx} \tag{44}$$

The perpendicular absorption coefficient $\alpha_\perp$ is the fractional change in the wave power per unit length along the direction of propagation. It is proportional to the density of power absorbed (20). The contributions of each harmonic to $\alpha_\perp$ can be separately calculated and the total absorption coefficient is $\alpha_\perp = \sum_{n=-\infty}^{+\infty} \alpha_{\perp n}$.

We consider an EBW approaching the nth harmonic of the EC resonance in a plasma where the harmonics do not overlap. In other words, the Doppler-broadened resonances are spatially isolated and only the $\alpha_{\perp n}$ contribution to the absorption coefficient is significant. This also assumes that if the wave is midway between the n and $(n \pm 1)$ harmonic resonances there is no damping of the wave. It is further assumed that the wave damps before reaching the location of the resonance so that the LFS and HFS approaches to the resonance can be considered separately. These assumptions will be justified *a posteriori* using numerical results. Without loss of generality we can then assume that the nth harmonic of the EC resonance is located at $x = 0$ and the EBW is approaching the resonance from $x = -\infty$.

From (44)

$$\frac{dS_\perp}{dx} + \alpha_{\perp n}S_\perp = 0 \tag{45}$$

with the initial condition $S_\perp (x \to -\infty) = S_{\perp 0}$ where $S_{\perp 0}$ is the incident energy flow density. For $x \leq 0$ we can formally integrate (45) to obtain

$$S_\perp (x) = S_{\perp 0} \exp\left[-\int_{-\infty}^{x} \alpha_{\perp n} (x')\ dx' \right] \tag{46a}$$

$$P (x) = S_{\perp 0}\alpha_{\perp n} (x) \exp\left[-\int_{-\infty}^{x} \alpha_{\perp n} (x')\ dx' \right] \tag{46b}$$

The power deposition profile $P(x)$ results from the balance between an increasing absorption coefficient and a decreasing power flow density as the wave propagates toward the resonance. The point $x = x_p$ $(-\infty < x_p < 0)$ where $P(x)$ will have a maximum is obtained from

$$\left.\frac{d\alpha_{\perp n}}{dx}\right|_{x=x_p} = \alpha_{\perp n}^2 (x_p) \tag{47}$$

The width of the deposition region is defined as $\Delta x = |x_2 - x_1|$ where x_1 and x_2 are given by

$$\begin{aligned} S_\perp (x_1) &= (1 - \delta) S_{\perp 0} \\ S_\perp (x_2) &= \delta S_{\perp 0} \end{aligned} \tag{48}$$

Here $\delta = [1 - \text{erf} (1)]/2 \simeq 0.08$ is such that 84% of the power is absorbed in the deposition region. If the deposition profile had a Gaussian shape, x_1 and x_2 would be the positions such that $P(x_1) = P(x_2) = e^{-1}P(x_p)$.

From (39) and (41) an expression for $\alpha_{\perp n}$ (23) is obtained for electrostatic waves in the weak damping and weakly relativistic approximations

$$\alpha_{\perp n} = \sqrt{\frac{\pi}{2}} \frac{\omega}{c} \frac{1}{|n_\parallel| \beta_T^2} \frac{\Gamma_n(\lambda_\perp)}{\lambda_\perp \Phi_\perp(\omega/\omega_c, \lambda_\perp)} e^{-\frac{p_n^2}{2}} \tag{49}$$

As shown in Section III, $\lambda_\perp$ and $\Phi_\perp(\omega/\omega_c, \lambda_\perp)$ are essentially independent of the electron density. Thus, $\alpha_{\perp n}$ is also independent of the electron density. This property reflects the electrostatic nature of EBWs. For higher densities there are more electrons interacting with the wave. However, for a fixed energy flow density, the electric field amplitude is smaller as there are more energy carriers.

Since $\lambda_\perp$ and $\Phi_\perp(\omega/\omega_c, \lambda_\perp)$ are also independent of temperature, the variations of $\alpha_{\perp n}$ with β_T scales approximately as

$$\alpha_{\perp n} \propto \frac{1}{\beta_T^2} e^{-\frac{p_n^2}{2}} \tag{50}$$

In the deposition region $p_n^2 \gg 1$ so that the temperature dependence of $\alpha_{\perp n}$ is dominated by the dependence on p_n. Assuming that EBWs damp sufficiently close to the nth harmonic resonance so that $|1 - y_n| \ll 1$ in the deposition region, the variation of $p_n(x)$ is essentially determined by the variation of the magnetic field. Thus, if the deposition region is narrow as compared to L, the power deposition profile can be approximately determined by ignoring the variations in the electron density and temperature. Also, we can reasonably assume that the magnetic field varies linearly in the vicinity of an EC harmonic resonance

$$\frac{dB}{dx} = \frac{\sigma B(0)}{L} \tag{51}$$

where $\sigma = +1$ for a LFS approach ($y_n < 1$) and $\sigma = -1$ for a HFS approach ($y_n > 1$).

A. Deposition profile in momentum space

The position of power deposition in momentum space is characterized by p_n, defined in section II E, which is the point on the resonance curves closest to the origin. Consequently, the relation between deposition profiles in momentum and configuration spaces is determined from the variations in p_n as a function of x

$$\frac{dp_n}{dx} \simeq -\frac{\sigma}{\beta_T n_\parallel L} \tag{52}$$

From (46a) and (49), and transforming to the momentum space coordinates using (52)

$$S_\perp(p_n) = S_{\perp 0} \exp\left[-\int_{|p_n|}^\infty \sqrt{\frac{2}{\pi}} \tau_{n\sigma}(p_n') e^{-|p_n'|^2/2} \, d|p_n'|\right] \tag{53}$$

with

$$\tau_{n\sigma}(p_n) = \frac{\pi}{2} \frac{L\omega}{c} \frac{1}{\beta_T} \frac{\Gamma_n(\lambda_\perp)}{\lambda_\perp \Phi_\perp} \tag{54}$$

Using (47) and (52), the position in momentum space p_{np} of the peak of the power deposition profile is obtained from

$$\left.\frac{d\alpha_{\perp n}}{dp_n}\right|_{p_n = p_{np}} = -\sigma L \beta_T n_\parallel \alpha_{\perp n}^2(p_{np}) \tag{55}$$

We assume that the variation of $\tau_{n\sigma}$ within the power deposition region does not affect the deposition profile. In other words, the variation in the integrand of (53) is dominated by the exponential term. Assuming $\tau_{n\sigma}(p_n) \simeq \tau_{n\sigma}(p_n = p_{np}) \equiv \tau_{n\sigma}^p$, (53) reduces to

$$S_\perp(p_n) \simeq S_{\perp 0} \exp\left[-\tau_{n\sigma}^p\left(1 - \text{erf}\left[\frac{|p_n|}{\sqrt{2}}\right]\right)\right] \tag{56}$$

Then from (55)

$$|p_{np}| = \sqrt{\frac{2}{\pi}} \tau_{n\sigma}^{p} \exp\left[-\frac{|p_{np}|^2}{2}\right] \tag{57}$$

In (56) the parameter $\tau_{n\sigma}^{p}$ can be interpreted as the optical depth of the nth harmonic resonance for a LFS approach ($\sigma = +1$) or a HFS approach ($\sigma = -1$). For larger $\tau_{n\sigma}^{p}$ the wave power is deposited farther away from the origin in momentum space and, thus, on more energetic electrons.

The LFS and HFS deposition profiles are shown in Fig.7 as a function of p_n at the first and second harmonic, respectively. The profiles obtained from (53) and (56) are compared to the profiles calculated using R2D2. The good agreement between these results justifies our approximations including the assumption that $\tau_{n\sigma}$ is constant within the deposition region.

The momentum space positions corresponding to x_1 and x_2, namely p_{n1} and p_{n2}, are determined from (48) and (56). In Fig.8 the values of p_{n1}, p_{n2} and p_{np} (57) are plotted as a function of $\tau_{n\sigma}^{p}$. For $\tau_{n\sigma}^{p} \ll 1$, $|p_{np}| \simeq \sqrt{2/\pi}\tau_{n\sigma}^{p}$ varies linearly with $\tau_{n\sigma}^{p}$. For $\tau_{n\sigma}^{p} \gg 1$, $|p_{np}|$ varies slowly with $\tau_{n\sigma}^{p}$.

Figure 9 shows τ_{1+} and τ_{2-} as a function of ω/ω_c between the first and second harmonic. The lines denoted by x_1, x_2, and x_p correspond to p_{n1}, p_{n2}, and p_{np}, respectively. In the deposition region the variations in τ_{1+} and τ_{2-} are weak, thereby validating the assumption that $\tau_{n\sigma}$ is constant within this region. The large values of $\tau_{n\sigma}^{p}$ imply that EBWs are completely absorbed before reaching the resonance. From Fig.8, we find that the power is mostly deposited on supra-thermal electrons. The width of the deposition profile $\Delta p_n = |p_{n2} - p_{n1}|$ is independent of $\tau_{n\sigma}$ and $\Delta p_n \simeq 1$. The location of the peak of deposition is weakly dependent on $\tau_{n\sigma}$ but strongly dependent on the shape of the distribution function. This is different from the deposition profiles of the X and O modes. For these modes $\tau_{n\sigma}$ is much smaller than for EBWs and the wave power is damped on thermal electrons. Also, the peak of the deposition profile is determined primarily by $\tau_{n\sigma}$.

The position of the peak of deposition in normalized momentum space p_{np} is calculated for various values of β_T and $|n_{\parallel}|$. Contours of constant $|p_{np}|$ are shown in Fig.10 for the LFS and the HFS cases. Over a broad range of β_T and $|n_{\parallel}|$, $|p_{np}|$ does not vary much. This is to be expected as $|p_{np}|$ is a slowly varying function of $\tau_{n\sigma}^{p}$. The power is deposited on suprathermal electrons with $3 \lesssim |p_{np}| \lesssim 4$.

In Fig.10 the limits of validity of the model are also shown. The limit for large $\beta_T |n_{\parallel}|$ in the upper right corners comes from harmonic overlapping where it is impossible to separate LFS deposition from HFS deposition. The condition for no overlap between the harmonics n and $n + 1$ is

$$|n_{\parallel}| \beta_T \lesssim \frac{1}{(2n + 1) |p_{np}|} \tag{58}$$

For small $|n_{\parallel}|$ and LFS deposition, corresponding to the upper left hand corner in Fig.10(a), (31) is not satisfied for $p_n = p_{np}$. For small $\beta_T |n_{\parallel}|$ and HFS deposition, corresponding to the lower left hand corner in Fig.10(b), the Z function expansion used in (40) is not valid.

In order to establish the effect of higher harmonics on the wave, the location $|p_{np}|$ of the power deposition in momentum space is calculated as a function of $|n_{\parallel}|$ for different harmonic numbers. The results in Figs.11(a) and 11(b) corresponding to LFS and HFS deposition, respectively, show that $|p_{np}|$ does not vary much with the harmonic number. However, the range of accessible $|n_{\parallel}|$ becomes more restricted at higher harmonics, in accordance with (58).

We find that the deposition occurs where $|\zeta_n| \gtrsim 2$, except for HFS absorption when $\beta_T |n_{\parallel}|$ becomes too small. Thus, the weak damping assumption and the large argument expansion of the plasma dispersion function used in our calculations are valid approximations.

B. Deposition profile in configuration space

The peak location x_p and width Δx of the profile in configuration space are related to $|p_{np}|$ and Δp_n. In the weakly relativistic approximation, expressions for the configuration space profile characteristics are derived using (35)

$$\frac{-x_p}{L} \simeq \beta_T |n_{\parallel}| |p_{np}| \left(1 - \sigma \frac{\beta_T |p_{np}|}{2 |n_{\parallel}|}\right) \tag{59a}$$

$$\frac{\Delta x}{L} \simeq \beta_T |n_{\parallel}| \Delta p_n \left(1 - \sigma \frac{\beta_T |p_{np}|}{|n_{\parallel}|}\right) \tag{59b}$$

The leading order term in (59a) is the Doppler shift from the resonance located at $x = 0$ and is proportional to $\beta_T \left| n_\parallel \right| \left| p_{np} \right|$. From (58) $0 \leq \left| x_p \right| / L \lesssim 1 / (2n + 1)$. The second term in (59a) is the relativistic correction to the Doppler shift. The relativistic shift is positive for the HFS approach ($\sigma = -1$) and the deposition occurs farther away from the resonance. It is negative for the LFS approach ($\sigma = +1$) and the deposition occurs closer to the resonance. The leading term in (59b) describes the Doppler broadening of the profile. The second term in (59b) is the relativistic correction. It leads to a broadening of the deposition profile for the HFS approach, and a narrowing of the deposition profile for the LFS approach to the resonance.

V. CONCLUSION

In this paper a linear analytical description of electron Bernstein waves has been developed in the weak damping, weakly relativistic, and electrostatic approximations. These approximations are substantiated by comparing the results from our model with the exact numerical results obtained from the code R2D2. The agreement between these calculations justifies our approximations.

The electrostatic nature of EBWs is revealed by its polarization which is mostly longitudinal (along the wave vector). Also, the perpendicular energy flow density is proportional to the density of the electrons and their thermal velocity. This is a characteristic of electrostatic waves for which the energy is primarily in the coherent motion of the particles rather than in the electromagnetic fields.

The dispersion characteristics are described by the real part of the wave vector $k_{\perp r}$ normalized to the electron Larmor radius ρ_T. To a good approximation $k_{\perp r} \rho_T$ is independent of the electron temperature, electron density, and the parallel index of refraction of the wave. However, the dispersion characteristics vary strongly with the magnetic field. In particular, $k_{\perp r} \rho_T > 1$ on the low-field side of the cyclotron resonances while $k_{\perp r} \rho_T < 1$ on the high-field side. For a given perpendicular energy flow, the electric field amplitude is much larger for waves propagating on the LFS than for waves propagating on the HFS of a resonance. Thus, the resonant interaction of EBWs with electrons is stronger for the LFS approach to a resonance.

Analytical calculations of wave characteristics in the weakly relativistic approximation were carried out for obliquely propagating waves with $\left| n_\parallel \right| \gg \beta_T$. The leading order relativistic corrections to the EBW dispersion relation, its polarization, and its energy flow density are of order β_T^2. Thus, these EBW propagation characteristics can be determined from the non-relativistic form of the dielectric tensor. However, relativistic corrections affect the resonant interaction of EBWs with electrons through the relativistic shifts and curvature of the resonance curves in momentum space. The calculation of wave damping must include these relativistic effects. The density of power absorbed is found to depend essentially on p_n, the point on the resonance curve that is closest to the origin in momentum space. This point is located on the $p_\perp = 0$ axis and corresponds to the highest phase space density on the resonance curve in a Maxwellian plasma.

The deposition profile for EBWs is evaluated in a slab geometry model and is found to be well localized in both configuration and momentum spaces. The EBWs are completely damped on electrons well before reaching any EC harmonic resonance. The power is deposited on suprathermal electrons with parallel momenta between 3 and 4 times the thermal momentum. Since more energetic electrons are less collisional, EBWs have the potential for efficient current drive. In configuration space the deposition profile is shifted and broadened by Doppler and relativistic effects.

The EBW characteristics determined from the linear description presented in this paper provide an insight into the interaction of EBWs with electrons. These properties will be useful in understanding the quasilinear diffusion of electrons interacting with EBWs, and for determining means of efficient current drive by EBWs.

Acknowledgments

APPENDIX A: WEAKLY RELATIVISTIC DESCRIPTION OF ELECTROSTATIC WAVES

In the weak damping approximation, the electrostatic dispersion relation (29) and density of power absorbed (30) can be derived from

$$\begin{aligned} D_{\mathrm{L}} &= \mathrm{Re}\left[F_{\mathrm{L}}\left(\omega, \mathbf{n} \right) \right] \\ \overline{P}_{\mathrm{L}} &= \mathrm{Im}\left[F_{\mathrm{L}}\left(\omega, \mathbf{n} \right) \right] \end{aligned} \tag{A1}$$

where **n** is real and

$$F_{\mathrm{L}}\left(\omega,\mathbf{n}\right) = 1 - \frac{\omega_p^2}{\omega^2}\left\langle \sum_{n=-\infty}^{+\infty} \frac{J_n^2}{\gamma\left(n_\parallel^2 + n_\perp^2\right)\beta_T^2}\frac{\left(y_n + n_\parallel\beta_T p_\parallel\right)^2}{\left(\gamma - n_\parallel\beta_T p_\parallel - y_n\right)}f_0\right\rangle \tag{A2}$$

For a relativistic Maxwellian (33),

$$F_{\mathrm{L}}\left(\omega,\mathbf{n}\right) = 1 + \frac{\omega_p^2}{\omega_c^2}\frac{1}{\lambda}\sum_{n=-\infty}^{+\infty}\int_0^{+\infty} dp_\perp p_\perp J_n^2 e^{-\frac{p_\perp^2}{2}}\mathcal{I}_n\left(p_\perp\right) \tag{A3}$$

where $\mathcal{I}_n$ includes all relativistic effects and is of the form

$$\mathcal{I}_n = -\frac{R\left(\beta_T\right)}{\sqrt{2\pi}}\int_{-\infty}^{+\infty}\frac{dp_\parallel}{\gamma}\frac{\left(y_n + n_\parallel\beta_T p_\parallel\right)^2}{\left(\gamma - n_\parallel\beta_T p_\parallel - y_n\right)}e^{-\frac{(\gamma-1)-\beta_T^2 p_\perp^2/2}{\beta_T^2}} \tag{A4}$$

1. Weakly relativistic approximation

In the weakly relativistic regime where $\beta_T \ll 1$

$$\gamma = 1 + \frac{\beta_T^2}{2}\left(p_\perp^2 + p_\parallel^2\right) + \mathcal{O}\left(\beta_T^4\right) \tag{A5}$$

$$R\left(\beta_T\right) = 1 + \mathcal{O}\left(\beta_T^2\right) \tag{A6}$$

Neglecting terms of order β_T^2 and higher,

$$\mathcal{I}_n = 1 + y_n + \frac{\zeta_0}{\sqrt{\pi}}\int_{-\infty}^{+\infty}\frac{1}{\sigma_\parallel\zeta_\parallel - \zeta_n - \eta\left(\zeta_\perp^2 + \zeta_\parallel^2\right)}e^{-\zeta_\parallel^2}d\zeta_\parallel \tag{A7}$$

where $\zeta_\parallel = p_\parallel/\sqrt{2}$, $\zeta_\perp = p_\perp/\sqrt{2}$, $\eta = \beta_T/\left(\sqrt{2}\left|n_\parallel\right|\right)$ and $\zeta_n = \left(1 - y_n\right)/\left(\sqrt{2}\left|n_\parallel\right|\beta_T\right)$. Equation (A7) can be rewritten as

$$\mathcal{I}_n = 1 + y_n - \frac{\zeta_0}{\eta\sqrt{\pi}\left(\zeta_+ - \zeta_-\right)}\left[\int_{-\infty}^{+\infty}\frac{1}{\sigma_\parallel\zeta_\parallel - \zeta_+}e^{-\zeta_\parallel^2}d\zeta_\parallel - \int_{-\infty}^{+\infty}\frac{1}{\sigma_\parallel\zeta_\parallel - \zeta_-}e^{-\zeta_\parallel^2}d\zeta_\parallel\right] \tag{A8}$$

where

$$\begin{aligned}\zeta_+ &= \frac{\eta^{-1}}{2} + \sqrt{\frac{\eta^{-2}}{4} - \left(\eta^{-1}\zeta_n + \zeta_\perp^2\right)}\\ \zeta_- &= \frac{\eta^{-1}}{2} - \sqrt{\frac{\eta^{-2}}{4} - \left(\eta^{-1}\zeta_n + \zeta_\perp^2\right)}\end{aligned} \tag{A9}$$

$\mathcal{I}_n$ can be expressed as a function of the plasma dispersion function Z

$$\mathcal{I}_n = 1 + y_n + \frac{\zeta_0}{\eta\left(\zeta_+ - \zeta_-\right)}\left[Z\left(\zeta_-\right) - Z\left(\zeta_+\right)\right] \tag{A10}$$

2. Non-relativistic limit

In the non-relativistic limit $\eta \to 0$ and (A9) yields

$$\begin{aligned}\zeta_+^{\mathrm{NR}} &= \infty\\ \zeta_-^{\mathrm{NR}} &= \zeta_n\end{aligned} \tag{A11}$$

so that from (A10)

$$\mathcal{I}_n^{\mathrm{NR}} = 1 + y_n + \zeta_0 Z\left(\zeta_n\right). \tag{A12}$$

Also (A3) reduces to

$$F_{\mathrm{L}}^{\mathrm{NR}}(\omega, \mathbf{n}) = 1 + \frac{\omega_p^2}{\omega_c^2} \sum_{n=-\infty}^{+\infty} \frac{\Gamma_n(\lambda_\perp)}{\lambda} \left(1 + y_n + \zeta_0 Z(\zeta_n)\right) \tag{A13}$$

so that

$$D_{\mathrm{L}}^{\mathrm{NR}} = 1 + \frac{\omega_p^2}{\omega_c^2} \sum_{n=-\infty}^{+\infty} \frac{\Gamma_n(\lambda_\perp)}{\lambda} \left(1 + y_n + \zeta_0 \operatorname{Re}\left[Z(\zeta_n)\right]\right)$$

$$\overline{P}_{\mathrm{L}}^{\mathrm{NR}} = \sqrt{\pi} \frac{\omega_p^2}{\omega_c^2} \sum_{n=-\infty}^{+\infty} \frac{\Gamma_n(\lambda_\perp)}{\lambda} \zeta_0 e^{-\zeta_n^2} \tag{A14}$$

$D_{\mathrm{L}}^{\mathrm{NR}}$ is the usual non-relativistic electrostatic dispersion relation [17].

3. Obliquely propagating waves

For obliquely propagating waves with $\left|n_\parallel\right| \gg \beta_T$, $\eta \ll 1$. For harmonic numbers such that $|\zeta_n| \ll \eta^{-1}$, we have

$$\begin{aligned}\zeta_+ &= \eta^{-1} - \zeta_n + \mathcal{O}(\eta) \\ \zeta_- &= \zeta_n + \eta\left(\zeta_n^2 + \zeta_\perp^2\right) + \mathcal{O}(\eta^2)\end{aligned} \tag{A15}$$

By using these expressions and the Taylor expansion of the Z function, we obtain

$$\mathcal{I}_n = \mathcal{I}_n^{\mathrm{NR}} + \eta\zeta_0\left[1 + 2\zeta_n Z(\zeta_n) + \left(\zeta_n^2 + \zeta_\perp^2\right) Z'(\zeta_n)\right] \tag{A16}$$

The weak damping approximation is restricted to regions where $\zeta_n \gtrsim 2$. Using the large argument expansion of the Z function

$$\begin{aligned}Z(\zeta_n) &\simeq -\zeta_n^{-1}\left[1 + \zeta_n^{-2}/2 + \mathcal{O}\left(\zeta_n^{-4}\right)\right] + i\sqrt{\pi}e^{-\zeta_n^2} \\ Z'(\zeta_n) &\simeq \zeta_n^{-2}\left[1 + 3\zeta_n^{-2}/2 + \mathcal{O}\left(\zeta_n^{-4}\right)\right] - 2i\sqrt{\pi}\zeta_n e^{-\zeta_n^2}\end{aligned} \tag{A17}$$

then

$$\mathcal{I}_n = \mathcal{I}_n^{\mathrm{NR}} + \eta\zeta_0\left[\zeta_n^{-2}\left(\frac{1}{2} + \zeta_\perp^2\right) - 2i\sqrt{\pi}\zeta_n\left(\zeta_n^2 + \zeta_\perp^2\right)e^{-\zeta_n^2}\right] \tag{A18}$$

to the leading order in ζ_n^{-2}. For harmonic numbers such that $|\zeta_n| \gtrsim \eta^{-1}$, relativistic effects can be neglected altogether in (A7) and we obtain $\mathcal{I}_n \simeq \mathcal{I}_n^{\mathrm{NR}}$.

Substituting (A18) into (A3), we obtain

$$D_{\mathrm{L}} = D_{\mathrm{L}}^{\mathrm{NR}} - \frac{\omega_p^2}{\lambda\omega_c^2} \sum_{\substack{n=-\infty \\ |\zeta_n| \ll \eta^{-1}}}^{+\infty} \frac{\beta_T^2}{(1 - y_n)^2} \left(\frac{1}{2}\Gamma_n(\lambda_\perp) + \left[\lambda_\perp\Gamma_n(\lambda_\perp)\right]'\right) \tag{A19}$$

$$\overline{P}_{\mathrm{L}} = \sqrt{\frac{\pi}{2}} \frac{1}{\lambda\left|n_\parallel\right|\beta_T} \frac{\omega_p^2}{\omega_c^2} \sum_{\substack{n=-\infty \\ |\zeta_n| \ll \eta^{-1}}}^{+\infty} \left\{\Gamma_n(\lambda_\perp) - \frac{(1 - y_n)}{n_\parallel^2}\left[\lambda_\perp\Gamma_n(\lambda_\perp)\right]'\right\} e^{-\frac{p_n^2}{2}} \tag{A20}$$

where p_n is given by (35). The relativistic corrections to the dispersion relation and the density of power absorbed are, respectively, of order

$$\frac{\beta_T^2}{1 - y_n} = \frac{\beta_T}{n_\parallel p_{n0}}; \qquad \frac{(1 - y_n)}{n_\parallel^2} = \frac{\beta_T p_{n0}}{n_\parallel} \tag{A21}$$

The weak damping approximation is characterized by $|\zeta_n| \gtrsim 2$ and, consequently, by $|p_{n0}| \gtrsim 3$. Then the relativistic effect on the power absorption is larger than the effect on the dispersion relation by at least an order of magnitude.

Thus, it is a good approximation to ignore the relativistic effects in the dispersion relation of EBWs. A detailed description of the weakly relativistic effects on kinetic waves is given in [17].

_____

[1] R.A. Cairns and C.N. Lashmore-Davies, Phys. Plasmas **7**, 4126 (2000).
[2] A.K. Ram and S.D. Schultz, Phys. Plasmas **7**, 4084 (2000).
[3] H.P. Laqua *et al.*, Phys. Rev. Lett. **78**, 3467 (1997).
[4] V. Shevchenko, Y. Baranov, M. O'Brien, and A. Saveliev, Phys. Rev. Lett. **89**, 2650054 (2002).
[5] M. Ono *et al.*, Nucl. Fusion **44**, 452 (2004).
[6] R.-J. Akers *et al.*, Phys. Plasmas **9**, 3919 (2002).
[7] I.B. Bernstein, Phys. Rev. **109**, 10 (1958).
[8] T.H. Stix, Theory of Plasma Waves (McGraw-Hill, New-York, 1962).
[9] E. Lazzaro and A. Orefice, Phys. Fluids **23**, 2330 (1980).
[10] J. Preinhaelter and V. Kopecky, J. Plasma Phys. **10**, 1 (1973).
[11] H. Weitzner and D.B. Batchelor, Phys. Fluids **22**, 1355 (1979).
[12] F.R. Hansen, J.P. Lynov, and P. Michelsen, Plasma Phys. Cont. Fusion **27**, 1077 (1984).
[13] A.K. Ram, A. Bers, and C.N. Lashmore-Davies, Phys. Plasmas **9**, 409 (2002).
[14] G. Taylor *et al.*, Phys. Plasmas **11**, 4733 (2004).
[15] A.K. Ram, J. Decker, and Y. Peysson, J. Plasma Phys. **71**, 675 (2005).
[16] A. Bers, Plasma Physics - Les Houches (Gordon and breach Science Publishers, 1975) 128.
[17] M. Brambilla, Kinetic Theory of Plasma Waves (Oxford Science Publications, 1998).
[18] J. Decker, Electron Bernstein wave current drive modeling in toroidal plasma confinement (PhD thesis, M.I.T., Department of Electrical Engineering and Computer Science, 2005).
[19] C.F. Kennel and F. Engelmann, Phys. Fluids **9**, 2377 (1966).
[20] I. Lerche, Phys. Fluids **11**, 1720 (1968).
[21] I.P. Shkarofsky, Phys. Fluids **9**, 561 (1966).

Figure Captions

Figure 1: Parabolic resonance curves ($n_\parallel = 1$) in momentum space for (a) $y_n = 0.9$, and (b) $y_n = 1.1$ corresponding to the low-field and high-field sides, respectively, of the nth harmonic resonance.

Figure 2: (a) Real and (b) imaginary parts of the EBW dispersion characteristics $n_\perp$ as a function of ω/ω_c calculated from R2D2 using the full (solid lines) and the weakly dissipative (dashed lines) dispersion relations. The following typical ST plasma parameters are used: $\omega_p^2/\omega^2 = 10$, $\beta_T = 0.05$ and $n_\parallel = 1$.

Figure 3: EBW dispersion characteristics $k_\perp \rho_T$ calculated as a function of (a) ω/ω_c, (b) β_T, (c) $n_\parallel$, and (d) ω_p^2/ω^2, respectively. The remaining constant parameters are $\omega/\omega_c = 1.5$, $\beta_T = 0.05$, $n_\parallel = 1$ and $\omega_p^2/\omega^2 = 10$.

Figure 4: Polarization vector components in the (T_1, T_2, L) coordinate system, calculated for the parameters of Fig.3 as a function of (a) ω/ω_c, and (b) β_T. The thick and thin lines refer, respectively, to relativistic and non-relativistic calculations by the code R2D2. In the electrostatic approximation the polarization is purely longitudinal.

Figure 5: Normalized perpendicular energy flow $|\overline{S}_\perp|$ calculated for the parameters of Fig.3 as a function of (a) ω/ω_c, (b) β_T, (c) $n_\parallel$, and (d) ω_p^2/ω^2, respectively.

Figure 6: Density of power absorbed $\overline{P}$ calculated for the parameters of Fig.3 as a function of ω/ω_c.

Figure 7: (a) LFS and (b) HFS EBW power deposition profile at the first and second harmonic, respectively, calculated as a function of p_n for the parameters of Fig.3 assuming a linear variation of the magnetic field with $L = 1$ m and $\omega/(2\pi) = 14$ GHz.

Figure 8: Peak value of the power deposition profile p_{np} as a function of the optical depth $\tau_{n\sigma}^p$. The limits p_{n1} and p_{n2} of the deposition profile are also represented.

Figure 9: Optical depth $\tau_{n\sigma}$ calculated for the parameters of Fig.7 as a function of ω/ω_c between the first and second harmonics.

Figure 10: Position of the peak of deposition $|p_{np}|$ in momentum space calculated for various values of β_T and $|n_\parallel|$ for (a) LFS and (b) HFS depositions. The remaining constant parameters are the same as in Fig.7.

Figure 11: Position $|p_{np}|$ of the peak of the deposition profile in momentum space calculated as a function of $|n_\parallel|$ for different harmonic numbers and for (a) LFS and (b) HFS depositions. The remaining constant parameters are the same as in Fig.7.
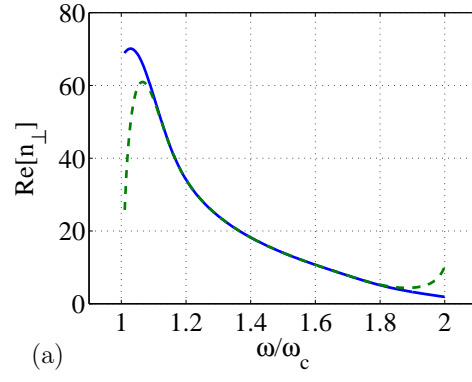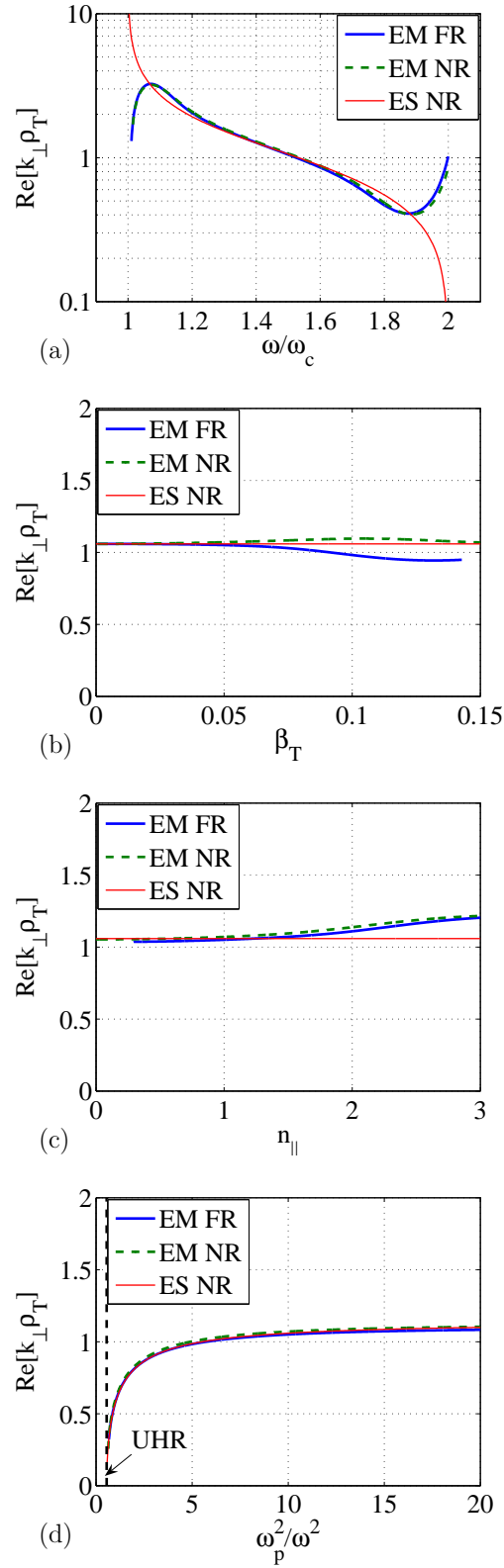
FIGURES
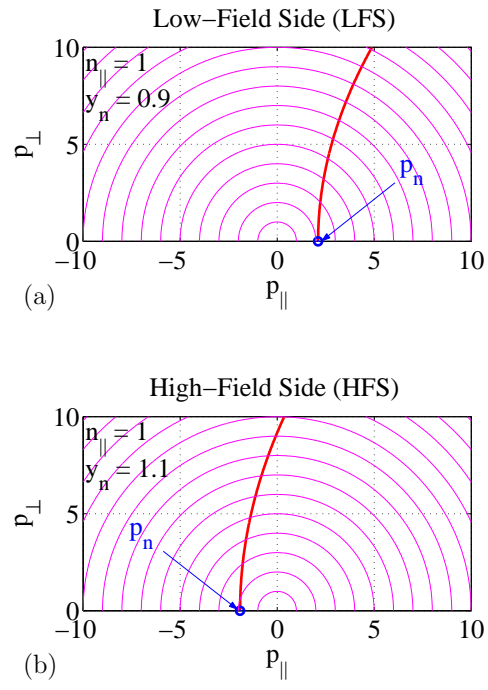
FIG. 1:

FIG. 2:

FIG. 3:

FIG. 4:

(a)

(b)

(c)

(d)

FIG. 5:

FIG. 6:

(a)

(b)
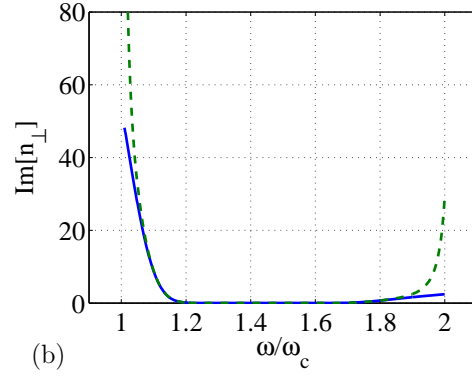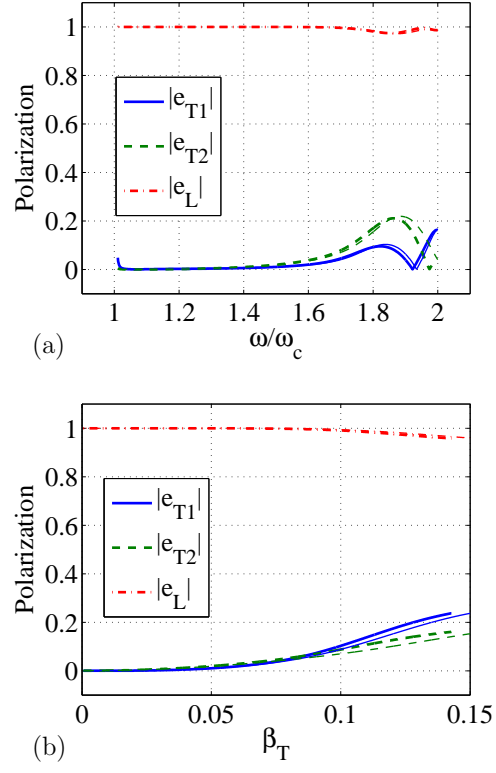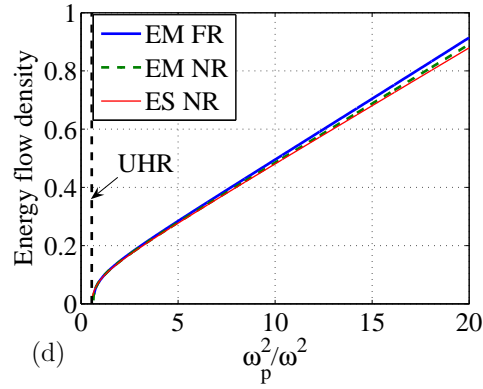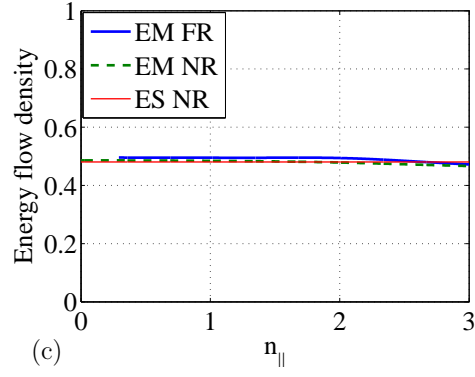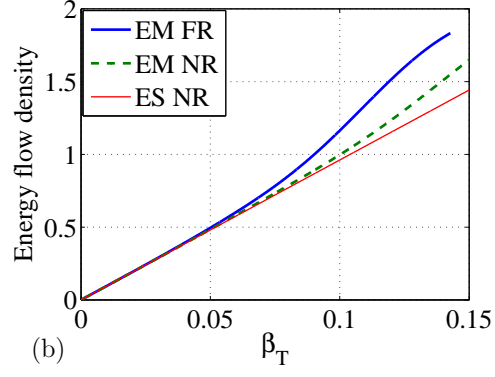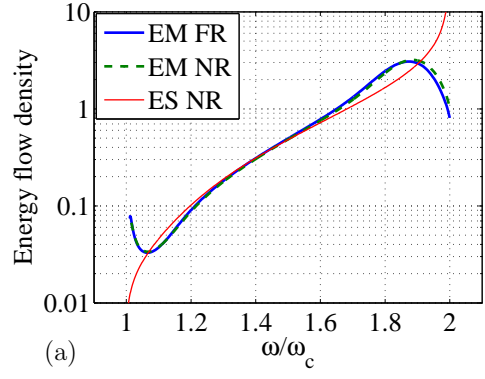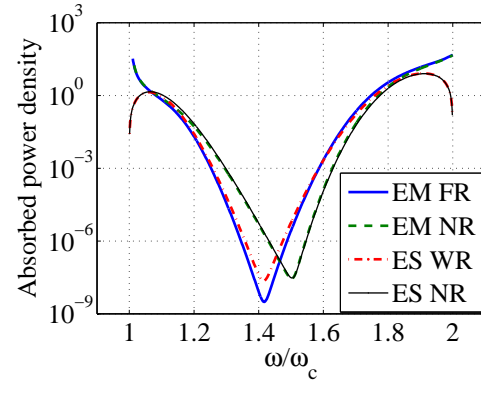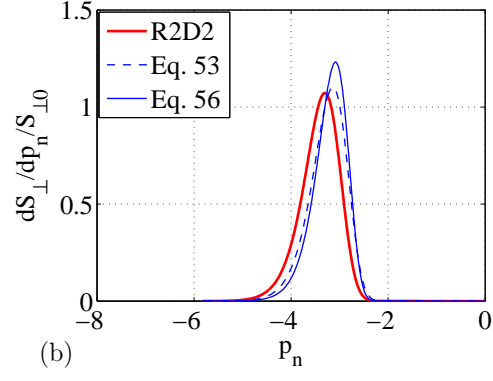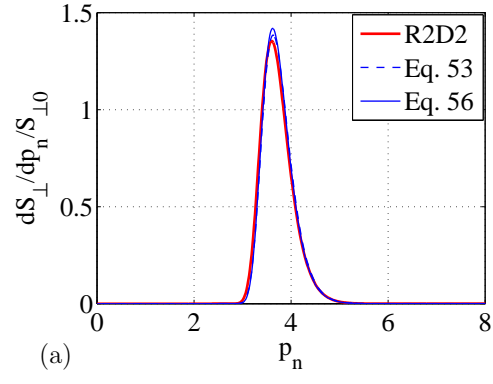
FIG. 7:

FIG. 8:

FIG. 9:

FIG. 10:

FIG. 11: